

# Stability of a DC Microgrid with a Nonlinear Nested Control Framework: The Fast Communication Scenario

Cornelia Skaga, *Graduate Student Member, IEEE*,

Mahdieh S. Sadabadi, *Senior Member, IEEE*, and Gilbert Bergna-Diaz, *Member, IEEE*

**Abstract**—As modern power systems continue to evolve into multi-agent, converter-dominated systems that demand reliable, stable, and optimal control architectures within an expandable framework, this paper investigates *scalable* stability guarantees of a promising *nonlinear* communication-reliant control framework for DC microgrids. Particularly, relying on *nested* control loops—inner decentralized/primary and outer distributed/secondary—the control configurations are designed to simultaneously achieve proportional current sharing and voltage containment within pre-specified limits, at the converged steady state. By enforcing sufficient time-scale separation at the border between the control loops, the system admits a singular perturbation formulation, allowing global exponential stability (G.E.S.) to be established via Lyapunov arguments. Although the theoretical G.E.S. certificate is structurally *scalable*, the stability guarantees depends on a sufficiently large *permanent* leakage—introduced in the primary controller. Thus, the results of this paper emphasize the importance of appropriate *practical* tuning guidelines and electrical parameter selection. The effectiveness of the proposed method is validated through case studies on a low-voltage DC microgrid under load variations and topological changes (and communication time-delays), followed by a small-signal stability analysis.

**Index Terms**—Converter-dominated grids, distributed cooperative control, nonlinear dynamics, optimal steady state operations.

## I. INTRODUCTION

In recent years, electric power systems have undergone a significant transition from conventional fossil-fuel-based generation toward the integration of small-scale distributed generation (DG) units such as photovoltaics, wind turbines, and battery energy storage systems, effectively interfaced through power electronic converters (PECs) [1], [2]. Driven by this transformation, modern power grids are evolving into converter-dominated, multi-agent systems ascribed by their efficient and reliable power management and control strategies [1], [3]. Particularly, given by the electrical characteristics of DGs and modern power electronic loads, such as electric vehicle chargers, DC MGs—defined as geographically decentralized, clustered low-voltage distribution systems—are increasingly recognized as a promising architecture for coordinating multiple converter-interfaced DGs, energy storage systems, and loads within flexible and continuously expandable energy networks [4], [5]. Moreover, microgrid architectures offer significant operational advantages through their ability to operate in both grid-connected mode—where the microgrid is connected to a larger transmission or distribution system—and autonomous islanded mode, in which the microgrid operates independently under a control architecture that enables coordinated and cooperative operation [4]. Such functionality

provides a safety mechanism during outages or large disturbances in the utility grid and supports the deployment of DC MGs in industrial applications, including isolated shipboard power systems, marinas and large ports with flexible loads, aircraft, and electric vehicles [4]–[8].

### A. Literature Review and Research Gap

Recent advances in control theory have shifted control architectures from traditional centralized schemes toward more flexible, scalable and reliable, distributed frameworks that leverage peer-to-peer communication among neighboring units for coordinated decision-making and optimal system operation in accordance with the specified control objectives [9]. Moreover, the low electrical inertia and weak damping characteristics of PEC-dominated systems increase the vulnerability to transient disturbances and reduce robustness against random perturbations, which further motivates the adoption of efficient and reliable distributed control structures in DC MGs [10]. Typically, such distributed architectures follow a hierarchical structure organized into primary, secondary, and tertiary control levels, enabling a certain degree of independence between control layers [11]. Within this framework, proper voltage regulation and proportional load (power or current) sharing are commonly defined as the primary control objectives for DC MGs. Voltage regulating is typically enforced through primary PEC controllers—regulating deviations in voltage and/or current (power) outputs relative to a reference value to ensure local voltage stability and reliable network operation [11]–[14]. These reference signals are provided by the secondary controller, which commonly employ digital communication links among active agents and consensus-based protocols to cooperatively restore nominal operating conditions; dealing with voltage compensation or power sharing performance, for coordinated operations across the microgrid [11], [12], [15]. Consequently, in DC MGs—comprising DGs with heterogeneous capacities—the secondary controller enables proportional power sharing, in which the active sources contribute power in proportion to their respective capacities [16].

However, without adequate time-scale separation, adverse interactions may arise between the primary and secondary control loops [4]. Accordingly, to enable scalable plug-and-play (PnP) functionality and ensure stable, reliable operation of DC MGs—in line with the specified control objectives—while adapting in real time to unknown and variable loads—distributed control structures commonly employ time-scale and bandwidth separation among the primary and secondary control layers [4], [11]. Recent research has introduced various distributed cooperative control frameworks for DC MGs [9], [13], [14], [17]–[20]—and references therein—demonstrating the feasibility of achieving simultaneous current sharing and *average voltage regulation*. However, average voltage regulation may lead to significant deviations in individual generator voltages, potentially exceeding operational limits [2]. To overcome this limitation, [2] introduces a novel

The preliminary results of this paper are presented in [1] Cornelia Skaga (corresponding author), and Gilbert Bergna-Diaz are with the Department of Electric Energy, Norwegian University of Science and Technology (NTNU), 7491 Trondheim, Norway (e-mail: cornelia.skaga@ntnu.no; gilbert.bergna@ntnu.no). Mahdieh S. Sadabadi is with the Department of Electrical and Electronic Engineering, The University of Manchester, M13 9PL, Manchester, UK (e-mail: mahdieh.sadabadi@manchester.ac.uk).

nonlinear distributed control framework with *nested* control loops—inner/primary controller and outer/secondary controller. The controller ensures that all energized units contribute power proportionally to their rated capacities while consistently operating within predefined voltage limits. However, the method proposed in [2] lacks a rigorous stability guarantee. Moreover, a closely related control architecture was proposed for AC grids in [3], along with a proof of global asymptotic stability. This proof leveraged singular perturbation theory (SPT) to separate the *nested* control loops by sufficient time-scales, enabling scalable stability conditions under reasonable assumptions for AC systems. In conventional AC MGs, the primary control layer operates at the fastest time-scale with the highest bandwidth, enabling near-instantaneous response to local disturbances, whereas the secondary controller operate at slower time-scales—typically on the order of minutes—with lower bandwidth requirements [11], [21]. However, in some methods [3], [22], [23] inverters are typically controlled to emulate the droop characteristics of slow synchronous generators [4]. Hence, the proof in [3] relies on assuming that the inner-loop controller (primary control of the inverters) behaves as decentralized slow virtual synchronous machines, operating at a slower time-scale than the distributed communication-reliant secondary controller. However, to the best of the authors knowledge, there are no standardized time-scale requirements for the control levels in DC systems, and given the natural *structural* differences between AC and DC grids, assuming similar time-scale separations may arguably be counter-intuitive. Hence, it is not entirely obvious that the stability conditions in [3] still hold *mutatis mutandis* in the DC grid case in [2].

### B. Contribution

Motivated by the proposed control approaches in [2] and [3], this paper aims to establish scalable global exponential stability (GES) guarantees for a DC microgrid with a distributed control architecture similar to [2]. The proposed analysis follows the methodology in [3], enforcing a time-scale separation with fast communication-based outer-loop (secondary) control dynamics and slower inner-loop (primary) control and electrical dynamics. Building upon the preliminary presented stability analysis in [1], this paper advances the technical results in the following ways: (i) we update the control dynamics to include a nonlinear and *non-permanent* leakage function of the decentralized inner-loop controller—for improved dynamical performance—and a *permanent* leakage to facilitate large signal stability guarantees, (ii) the stability proof has been substantially updated to accommodate these control modifications, and to guarantee G.E.S. in both saturated and unsaturated operations, (iii) we propose some *practical* guidelines for stability guarantees. Furthermore, the case studies are extended to empirically validate the theoretical assumptions for systems operating under the *practical* guidelines, and to evaluate whether the proposed controller consistently ensures voltage containment and convergence to a steady state ensuring proportional current sharing. The framework is also tested under communication time delays that both respect and violate the critical time-scale separation between nested control loops. Finally, a small-signal stability analysis is conducted to assess the potential for reducing the conservativeness of the large-signal stability result.

The rest of the paper is structured as follows. Section II presents the dynamical model of the electrical system and distributed control framework for a DC MG. In Section III, we present the

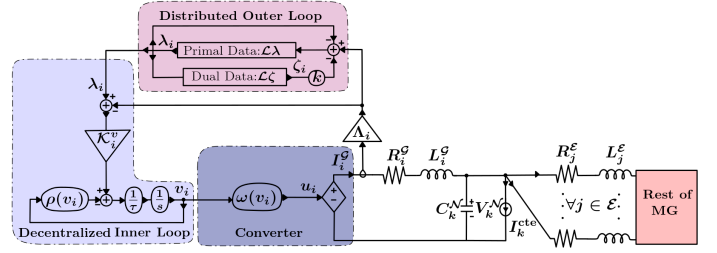


Fig. 1: DC microgrid dynamics - A single DG unit perspective.

main result of this paper: a comprehensive stability proof for a closed-loop DC microgrid with a nonlinear distributed controller, that under certain *practical* guidelines can stabilize to a desired steady state. Furthermore, in Section IV, the controller is evaluated via time-domain simulations on a 4-terminal low-voltage DC microgrid to demonstrate the effectiveness of the proposed method, including testing the performance under imposed time delays, followed by a small-signal stability analysis to complement the large-signal stability results. Finally, Section V concludes this paper.

## II. SYSTEM MODELING AND CONTROL FRAMEWORK

Throughout the paper, we use the following notations:  $\mathbb{R}^{n \times m}$  and  $\mathbb{R}^n$  denote a set of  $n \times m$  real matrices and  $n \times 1$  real vectors, respectively.  $\text{col}(\dots) \in \mathbb{R}^n$  denotes a column vector and  $\text{bcol}\{\dots\} \in \mathbb{R}^n$  denotes a column vector of vectors.  $\text{diag}(\dots) \in \mathbb{R}^{n \times n}$  denotes a diagonal matrix with scalar entries, and  $\text{bdiag}\{\dots\} \in \mathbb{R}^{n \times n}$  denotes a block diagonal matrix of vectors.  $0$  denotes a null matrix of appropriate dimensions, and  $\mathbb{I} = \text{diag}(1)$  denotes the identity matrix of appropriate dimensions.  $A|_{\text{sym}}$  denotes the symmetrical part of an arbitrary square matrix  $A \in \mathbb{R}^{n \times n}$ , defined as  $A|_{\text{sym}} = \frac{1}{2}(A + A^T)$ . Given a symmetric matrix  $X$ ,  $X \succ 0$  ( $X \succeq 0$ ) indicates that  $X$  is a positive-definite (positive semi-definite) matrix. Furthermore,  $x \gg y$  denotes that  $x$  is much larger than  $y$ , and  $\mathbb{R}_{\geq 0}$  defines all non-negative real values. Given a scalar or a vector  $x$ , the value at the equilibrium point is indicated as  $\bar{x}$ , and  $\tilde{x}$  denotes a shifted variable where  $\tilde{x} \triangleq x - \bar{x}$ . Note that  $\mathcal{G} = \{1, 2, \dots, n_i\}$  is the set of distributed generators,  $\mathcal{E} = \{1, 2, \dots, n_j\}$  is the set of power lines,  $\mathcal{N} = \{1, 2, \dots, n_k\}$  is the set of power consuming loads, and  $\mathcal{N}^c = \{1, 2, \dots, n_i\}$  is the set of neighboring communicating DGs.

### A. Dynamical model of Microgrids

The DC microgrid is based on the models presented in [24] and [2]. The agents are the distributed generators (DGs), located close to the power-consuming loads (ZI-loads), and are effectively interfaced with the rest of the MG through voltage-controlled converters. Due to the fast dynamics of power electronic converters, their equivalent zero-order models are considered in this paper. The DGs are interconnected both electrically and via distributed communication links, forming a cyber-physical grid. Graph theory is used to establish the physical and virtual interconnections—see Appendix A in [3] for the precise definitions of the included graphs. Following the model illustrated in Fig. 1, the electrical dynamics for

the  $i$ -th DG ( $i \in \mathcal{G}$ ), connected to the  $j$ -th power line ( $j \in \mathcal{E}$ ) and the  $k$ -th power-consuming load ( $k \in \mathcal{N}$ ) are presented in (1).

$$L_i^{\mathcal{G}} \dot{I}_i^{\mathcal{G}} = u_i - \sum_k b_{ik}^{\mathcal{G}} V_k^{\mathcal{N}} - R_i^{\mathcal{G}} I_i^{\mathcal{G}}, \quad (1a)$$

$$L_j^{\mathcal{E}} \dot{I}_j^{\mathcal{E}} = - \sum_k b_{jk}^{\mathcal{E}} V_k^{\mathcal{N}} - R_j^{\mathcal{E}} I_j^{\mathcal{E}}, \quad (1b)$$

$$C_k^{\mathcal{N}} \dot{V}_k^{\mathcal{N}} = \sum_j b_{kj}^{\mathcal{E}} I_j^{\mathcal{E}} + \sum_i b_{ki}^{\mathcal{G}} I_i^{\mathcal{G}} - G_k^{\text{cte}} V_k^{\mathcal{N}} - I_k^{\text{cte}}, \quad (1c)$$

where  $L_i^{\mathcal{G}}$ ,  $R_i^{\mathcal{G}}$ ,  $I_i^{\mathcal{G}}$ , and  $u_i$  are the inductance, parasitic resistance, current, and voltage of the  $i$ th DG, respectively. In (1b),  $L_j^{\mathcal{E}}$ ,  $R_j^{\mathcal{E}}$ , and  $I_j^{\mathcal{E}}$  are the inductance, resistance, and current of the  $j$ th power line, respectively. In (1c),  $C_k^{\mathcal{N}}$ ,  $V_k^{\mathcal{N}}$ ,  $G_k^{\text{cte}}$  and  $I_k^{\text{cte}}$  respectively are the shunt capacitance, its voltage, the constant conductance, and constant current of the  $k$ th power-consuming load. The elements  $b_{ik}^{\mathcal{G}}$  and  $b_{jk}^{\mathcal{E}}$  correspond to the incidence matrices, characterizing arbitrary current flows within the network. When current flows from the  $j$ -th power line to the  $k$ -th load, the matrix element  $b_{jk}^{\mathcal{E}}$  is set to 1, in the absence of current exchange  $b_{jk}^{\mathcal{E}} = 0$ , and for an opposite current flow  $b_{jk}^{\mathcal{E}} = -1$ . Similarly, the matrix element  $b_{ki}^{\mathcal{G}}$  characterizes current flows between DGs interconnected loads, however, we treat the DGs as power injection components, thus,  $b_{ik}^{\mathcal{G}} = -1$  is not considered.

### B. Nested Control Framework

Motivated by the *nonlinear* controller design in [2], this paper aims to modify the control configuration to guarantee convergence to steady state while ensuring simultaneous achievement of the following two control objectives in DC microgrids:

- voltage containment within pre-specified limits,
- proportional current sharing at steady state.

The voltage containment objective is required to hold uniformly for all admissible initial conditions and disturbances. These control objectives are mathematically formulated as follows:

$$\begin{aligned} V_{\min} \leq V_i^{\mathcal{G}}(t) \leq V_{\max}, \quad \forall t \in \mathbb{R}_{\geq 0}, \\ \lim_{t \rightarrow \infty} (I_i^{\mathcal{G}}(t)/I_i^{\text{rated}} - I_l^{\mathcal{G}}(t)/I_l^{\text{rated}}) = 0, \quad \forall i, l \in \mathcal{G}, i \neq l, \end{aligned} \quad (2)$$

where  $V_i^{\mathcal{G}}$  is the voltage output,  $I_i^{\text{rated}}$  is the rated current, and  $V_{\min}$  and  $V_{\max}$  are the lower and upper voltage bounds of the  $i$ -th DG. To achieve the objectives stated in (2), a nested control framework is proposed, which comprises of two control loops: a decentralized(/primary) inner-loop controller for voltage containment and a distributed(/secondary) outer-loop for proportional current sharing.

### C. Decentralized Inner-Loop Controller

The inner-loop controller is modeled as a local current controller of the converters, regulating current deviations relative to a reference set-point value generated by the outer-loop controller. It is implemented as an integral controller, augmented with a *non-permanent* nonlinear leakage function to ensure consistent system behavior and stable operation—thereby constituting the primary control layer. The inner-loop controller dynamics of the  $i$ -th DG are given by:

$$u_i = \omega(v_i) = V^* + \Delta \tanh(v_i / \Delta), \quad (3a)$$

$$\tau_i \dot{v}_i = -\rho(v_i) v_i + \mathcal{K}_i^v (\lambda_i - \Lambda_i I_i^{\mathcal{G}}), \quad (3b)$$

$$\rho(v_i) = \alpha (1 + 0.5 [\tanh(b(v_i - v_{\text{pos}})) - \tanh(b(v_i - v_{\text{neg}}))]), \quad (3c)$$

where  $V^* = \frac{1}{2}(V_{\min} + V_{\max})$  is the central point within the safe voltage range, and  $\Delta = \frac{1}{2}(V_{\max} - V_{\min})$  is the maximum allowed deviation from  $V^*$ . The integral controller state  $v_i$  enters the control input  $u_i$  of DG $_i$  through the nonlinear hyperbolic tangent function  $\omega(v_i)$ , saturating the controller state value whenever it exceeds predefined limits. In (3),  $\rho(v_i)$  is a nonlinear leakage operating as an anti-wind-up function when the system reaches voltage saturation under the given arguments;  $v_{\text{pos}} = \Delta \tanh^{-1}[(v_{\max} - v_{\text{tol}} - V^*)/\Delta]$  and  $v_{\text{neg}} = \Delta \tanh^{-1}[(v_{\min} + v_{\text{tol}} - V^*)/\Delta]$ , with  $v_{\text{tol}}$  being the saturation tolerance,  $\alpha$  is the leakage coefficient scaling the upper bound value, and  $b$  is implemented to scale the steepness of the curve.

### D. Distributed Outer-Loop Controller

The outer-loop controller is designed to restore nominal operating conditions—constituting the secondary control layer. The proposed control architecture is distributed, relying on communication among neighboring DGs to enforce the consensus of the primal and dual communication state variables. Motivated by the distributed control proposal in Section II.C in [2], the outer-loop controller dynamics of the  $i$ -th DG are given by:

$$\tau_i^p \dot{\lambda}_i = \Lambda_i I_i^{\mathcal{G}} - \lambda_i - \sum_{j \in \mathcal{N}^c} [a_{ij}(\zeta_i - \zeta_j) - k a_{ij}(\lambda_j - \lambda_i)], \quad (4a)$$

$$\tau_i^d \dot{\zeta}_i = \sum_{j \in \mathcal{N}^c} a_{ij}(\lambda_i - \lambda_j), \quad (4b)$$

with  $\lambda_i$  and  $\zeta_i$  are the primal and dual communicated states of the cyber network with respective time constants  $\tau_i^p$  and  $\tau_i^d$ . In (4),  $a_{ij}$  is the *adjacency matrix* element, characterizing the communication network topology,  $k$  is a positive gain, and  $\Lambda_i = 1/I_i^{\text{rated}}$ . In summary, this secondary controller is derived by means of the Lagrange multiplier method, where it ensures that the system stabilizes at an equilibrium—characterized by the primal and dual Karush–Kuhn–Tucker (KKT) conditions—which is the argument that minimizes a cost function. More precisely, the cost function was designed to ensure proportional current sharing at steady state across the DC MG, (see (2)). Consequently, each local optimizer of the outer-loop controller requires the rated current of the associated DG $_i$ .

### E. Closed-loop DC Microgrid Dynamics

Given DG dynamics in (1), the proposed decentralized inner-loop controller in (3), and distributed outer-loop controller in (4), the closed-loop microgrid dynamics in compact form are presented as follows:

$$L^{\mathcal{G}} \dot{I}^{\mathcal{G}} = \omega(v) - \beta^{\mathcal{G}} V^{\mathcal{N}} - R^{\mathcal{G}} I^{\mathcal{G}}, \quad (5a)$$

$$L^{\mathcal{E}} \dot{I}^{\mathcal{E}} = -\beta^{\mathcal{E}} V^{\mathcal{N}} - R^{\mathcal{E}} I^{\mathcal{E}}, \quad (5b)$$

$$C^{\mathcal{N}} \dot{V}^{\mathcal{N}} = \beta^{\mathcal{E}\top} I^{\mathcal{E}} + \beta^{\mathcal{G}\top} I^{\mathcal{G}} - G^{\text{cte}} V^{\mathcal{N}} - I^{\text{cte}}, \quad (5c)$$

$$\tau \dot{v} = -\rho(v) v + \mathcal{K}_v (\lambda - \Lambda I^{\mathcal{G}}), \quad (5d)$$

$$\tau_p \dot{\lambda} = \Lambda I^{\mathcal{G}} - \lambda - \mathcal{L} \zeta - k \mathcal{L} \lambda, \quad (5e)$$

$$\tau_d \dot{\zeta} = \mathcal{L} \lambda, \quad (5f)$$

with  $L^{\mathcal{G}} = \text{diag}(L_i^{\mathcal{G}}) \in \mathbb{R}^{n_i \times n_i}$ ,  $I^{\mathcal{G}} = \text{col}(I_i^{\mathcal{G}}) \in \mathbb{R}^{n_i}$ ,  $R^{\mathcal{G}} = \text{diag}(R_i^{\mathcal{G}}) \in \mathbb{R}^{n_i \times n_i}$ ,  $\omega(v) = \text{col}(\omega(v_i)) \in \mathbb{R}^{n_i}$ ,  $\beta^{\mathcal{G}} = [b_{ik}^{\mathcal{G}}] \in \mathbb{R}^{n_i \times n_k}$ ,  $L^{\mathcal{E}} = \text{diag}(L_j^{\mathcal{E}}) \in \mathbb{R}^{n_j \times n_j}$ ,  $I^{\mathcal{E}} = \text{col}(I_j^{\mathcal{E}}) \in \mathbb{R}^{n_j}$ ,  $R^{\mathcal{E}} = \text{diag}(R_j^{\mathcal{E}}) \in \mathbb{R}^{n_j \times n_j}$ ,  $\beta^{\mathcal{E}} = [b_{jk}^{\mathcal{E}}] \in \mathbb{R}^{n_j \times n_k}$ ,  $C^{\mathcal{N}} = \text{diag}(C_k^{\mathcal{N}}) \in \mathbb{R}^{n_k \times n_k}$ ,  $V^{\mathcal{N}} = \text{col}(V_k^{\mathcal{N}}) \in \mathbb{R}^{n_k}$ ,  $G^{\text{cte}} = \text{diag}(G_k^{\text{cte}}) \in \mathbb{R}^{n_k \times n_k}$ ,  $I^{\text{cte}} = \text{col}(I_k^{\text{cte}}) \in \mathbb{R}^{n_k}$ ,  $v = \text{col}(v_i) \in \mathbb{R}^{n_i}$ ,  $\tau = \text{diag}(\tau_i) \in \mathbb{R}^{n_i \times n_i}$ ,

$\rho(v) = \text{diag}(\rho(v_i)) \in \mathbb{R}^{n_i \times n_i}$ ,  $\mathcal{K}_v = \text{diag}(\mathcal{K}_i^v) \in \mathbb{R}^{n_i \times n_i}$ ,  $\lambda = \text{col}(\lambda_i) \in \mathbb{R}^{n_i}$ ,  $\Lambda = \text{diag}(\Lambda_i) \in \mathbb{R}^{n_i \times n_i}$ ,  $\zeta = \text{col}(\zeta_i) \in \mathbb{R}^{n_i}$ ,  $\tau_p = \text{diag}(\tau_i^p) \in \mathbb{R}^{n_i \times n_i}$ ,  $\tau_d = \text{diag}(\tau_i^d) \in \mathbb{R}^{n_i \times n_i}$ . Finally,  $\mathcal{L} = [l_{ij}] \in \mathbb{R}^{n_i \times n_i}$  is the *Laplacian* matrix, containing the consensus properties.

**Assumption 1.** *It is assumed that the communication network (represented by the Laplacian matrix  $\mathcal{L}$ ) is strongly connected and undirected.*

### III. SYSTEM STEADY STATE AND STABILITY ASSESSMENT

In this section, we aim to prove that the closed-loop DC MG system augmented with the proposed nested control framework in (5) exponentially converges to an equilibrium in which the two control objectives in (2) are simultaneously satisfied. To prove the stability of the closed-loop DC microgrid in (5) and to account for the nonlinear dynamics and nested control loops, singular perturbation theory (SPT) in Subsection III-B is first applied to separate the outer-loop and inner-loop dynamics (including the electrical dynamics) by a sufficient time-scale separation [25]. Lyapunov theory is then used in Subsection III-C to derive a *scalable* global exponential stability (G.E.S.) certificate for the closed-loop DC MG—provided that certain tuning conditions (and electrical specifications) are satisfied.

#### A. Equilibrium Analysis

To analyze whether the DC microgrid converges to a steady state that satisfies the two control objectives in (2), we begin by characterizing the equilibrium of (5). To this end, we derive the steady state algebraic equations of (5) by imposing  $\dot{x} = 0$  for all states. Hence, any steady state needs to satisfy:

$$0 = f(\bar{I}^G, \bar{I}^E, \bar{V}^N, \bar{v}, \bar{\lambda}, \bar{\zeta})$$

Under *Assumption 1*, we exploit the Laplacian property  $\mathcal{L}\mathbb{1} = 0$ . Consequently, the steady-state operation of the dual communication dynamics in (5f) enforces all DGs to cooperatively reach a consensus on the primal communicated state, i.e.,  $\bar{\lambda} = \lambda_s \mathbb{1}$ , where  $\lambda_s$  denotes the common consensus value. Considering the steady state operation of (5d)—when the voltages operate within the saturation limits; i.e., inactive leakage function  $\rho(\bar{v}) - \Lambda \bar{I}^G$  is forced equal to  $\bar{\lambda}$ . As a result, the primal communication dynamics in (5e) reach steady state when  $\bar{\zeta} = \zeta_s \mathbb{1}$ , where  $\zeta_s$  denotes the common consensus value, thereby guaranteeing consensus among the DGs with respect to the dual communicated state. The steady state of the electrical network (5a)–(5c) is consequently uniquely defined.

**Remark 1.** (Optimal Steady State) *Section III.1 in [16] shows that the DC microgrid converges to an optimal steady state when the primal and dual KKT conditions are satisfied, and saturation is avoided. Thus,  $\rho(\bar{v}) = 0$  ensures the strict proportional current-sharing condition;  $\Lambda \bar{I}^G = \bar{\lambda}$ , provided that all neighboring DGs collaboratively determine the a common consensus value for the primal and dual communication states, and as long as  $\rho(\bar{\lambda})$  is uniformly defined for all DGs. In contrast, during voltage saturation the non-permanent leakage function in (5d) activates,  $\rho(\bar{v}) \neq 0$ , which drives the MG to a another optimum that satisfies the KKT conditions, however diminished the strict proportional current-sharing condition. Note that the voltage containment objective is satisfied uniformly for all operating conditions and admissible initial configurations, enforced by the nonlinear hyperbolic tangent function  $\omega(v)$  in (3a).*

#### B. Time-Scale Separation of the Nested Control-Loops

To facilitate expressing the DC microgrid system as a singularly perturbed problem, the closed-loop system in (5) is separated into *slow* and *fast* subsystems under the time-scale separation assumption stated below:

**Assumption 2.** (Time-Scale Separation) *It is assumed that the outer-loop dynamics operates at a faster time-scale than the rest of the system dynamics. The outer-loops respective time constants ( $\tau_p, \tau_d$ ) are therefore assumed to be significantly smaller than the smallest time constant of the slow dynamics ( $\varepsilon$ ). Thus, we assume:  $\tau_p, \tau_d \ll \varepsilon$ , with  $\varepsilon$  assumed to be the time constant of the integral controller;  $\tau$ .*

Specifically, under *Assumption 2*, the DC microgrid dynamics in (5a)–(5d) constitute the slow subsystem  $s(\cdot)$ , whereas (5e)–(5f) represent the fast dynamics  $f(\cdot)$ —forming the two time-separated systems:

$$\dot{x} = s(x, z) \quad \text{and} \quad \varepsilon \dot{z} = f(x, z), \quad (7)$$

with  $x = \text{bcol}\{I^G, I^E, V^N, v\} \in \mathbb{R}^{2n_i + n_j + n_k}$  and  $z = \text{bcol}\{\lambda, \zeta\} \in \mathbb{R}^{2n_i}$ .

To further simplify the stability analysis, the order the outer-loop is preliminarily reduced using a method similar to [3]. The specific assumptions underlying this order reduction are detailed in the following.

**Assumption 3.** (Time-scales of the Outer-Loop) *The primal communication dynamics in (5e) is assumed to operate at a significantly faster time-scale than the dual communication dynamics in (5f)—characterized by the following time-scale assumption:  $\tau_p \ll \tau_d$ .*

Let *Assumption 3* hold, and assume that  $\tau_p \dot{\lambda} \approx 0$ . As a result, the primal communication state can be expressed as a function of the dual communication state, i.e.,  $\lambda = K_1 \Lambda I^G - K_1 \mathcal{L} \zeta$ , with a positive-definite matrix  $K_1 \triangleq [\mathbb{I} + k \mathcal{L}]^{-1} \succ 0$ , resulting in some added damping in the  $\zeta$  coordinate in (5f). Accordingly, the closed-loop DC MG dynamics—specifically (5d)–(5f)—are redefined as follows:

$$\tau \dot{v} = -\rho(v)v + \mathcal{K}_v (K_1 (\Lambda I^G - \mathcal{L} \zeta) - \Lambda I^G) - \mathcal{B}_v (v - v^*), \quad (8a)$$

$$\tau_d \dot{\zeta} = \mathcal{L} K_1 (\Lambda I^G - \mathcal{L} \zeta). \quad (8b)$$

Consequently, the two time-separated systems in (7) are now governed by the slow states  $x$  and the *reduced* fast state vector  $z^* = \text{col}(\zeta_i)$ ,  $\forall i \in \mathbb{R}^{n_i}$ :

$$\dot{x} = s(x, z^*) \quad \text{and} \quad \varepsilon \dot{z}^* = f(x, z^*). \quad (9)$$

Additionally, a *permanent* leakage term  $\mathcal{B}_v = \text{diag}(\mathcal{B}_i^v) \in \mathbb{R}^{n_i \times n_i}$  is introduced in the integral controller state coordinate in (8a) to introduce dissipation when the voltages operates within safe limits ( $\rho(v) = 0$ ), which is essential for the subsequent stability analysis, with  $v^*$  being the constant estimated value of  $v$  in steady state for the ideal nominal operating point.

**Assumption 4.** (Frozen Variables in the Boundary Layer System) *Let Assumptions 2 and 3 hold, and let*

$$h(x) = \text{bcol}\{h_i(x)\}, \quad \forall i \in \mathcal{N}_e,$$

*be the unique solution of  $\varepsilon \dot{z}^* = f(x, z^*)$  for  $\varepsilon \approx 0$ . Expressed in terms of incremental states, then gives*

$$H(\tilde{x}) \triangleq \text{bcol}\{h(x) - h(\bar{x})\} = \text{bcol}\{\hat{H}(\tilde{x}) - h(\bar{x})\},$$

with  $\tilde{x} = x - \bar{x}$ , and  $\hat{H}(\tilde{x}) = h(\tilde{x} + \bar{x})$ . Under Assumption 2, we assume that the slow states entering the fast dynamics can be treated as frozen variables. Thus, in the boundary layer system,  $x = \bar{x}$  and therefore  $\tilde{x} = 0$ , resulting in

$$\hat{H}(\tilde{x}) = h(\bar{x}) \rightarrow H(\tilde{x}) = \{h(\bar{x}) - h(\bar{x})\} = 0.$$

Moreover, let  $\tilde{y} \triangleq \text{bcol}\{\tilde{z}^* - h(\tilde{x})\}$  be the error between the actual fast dynamics ( $\tilde{z}^*$ ) and the quasi-steady state ( $h(\tilde{x})$ ). Under sufficient time-scale separation, we assume that  $\tilde{z}^* = h(\bar{x})$  such that  $\tilde{y} = 0$  in the boundary layer system. Thus, from the above expressions, we let

$$\tilde{z}^* = (y - \bar{y}) + (h(x) - h(\bar{x})) = \tilde{y}, \quad \text{with } y = \tilde{y} + \bar{y}.$$

**Theorem 1.** (Singularly Perturbed Problem) *Let Assumptions 1-4 hold. Consider the closed-loop dynamics of the reduced model in (9), and let*

$$\begin{aligned} \Omega(\tilde{v}) &\triangleq \omega(v) - \omega(\bar{v}), & \Gamma(\tilde{v}) &\triangleq \rho(v)v - \rho(\bar{v})\bar{v} \\ \tilde{x} &\triangleq \text{bcol}\{\tilde{I}^G, \tilde{I}^E, \tilde{V}^N\}, & \mathcal{P}_s &\triangleq \text{bdiag}\{R^G, R^E, G^{\text{cte}}\} \succ 0 \\ \mathcal{Q}_f &\triangleq \text{diag}(\tau_i^d) \succ 0, & \mathcal{P}_f &\triangleq \mathcal{L}K_1\mathcal{L} \succ 0 \\ \mathcal{Q}_s &\triangleq \text{bdiag}\{L_i^G, L_j^E, C_k^N\} \succ 0, & & \\ \mathcal{J}_s &\triangleq \begin{bmatrix} 0 & 0 & -\beta^G \\ 0 & 0 & -\beta^E \\ \beta^G \top & \beta^E \top & 0 \end{bmatrix}, & \kappa_1 &\triangleq \text{bdiag}\{\mathbb{I}, 0, 0\}. \end{aligned} \quad (10)$$

The two time-separated systems in (9) can then be expressed as the singular perturbed problem in (11) under the stretched timescale  $\mathbf{t} = (t/\varepsilon)$ :

$$\hat{s}(\tilde{x}, H(\tilde{x})) : \begin{cases} \mathcal{Q}_s \dot{\tilde{x}} = (\mathcal{J}_s - \mathcal{P}_s)\tilde{x} + \kappa_1 \Omega(\tilde{v}), \\ \tau \dot{\tilde{v}} = -\Gamma(\tilde{v}) + \mathcal{K}_v(K_1(\Lambda \tilde{I}^G - \mathcal{L}H(\tilde{x})) - \Lambda \tilde{I}^G) - \mathcal{B}_v \tilde{v}, \end{cases} \quad (11a)$$

$$\hat{f}(\tilde{y}) : \begin{cases} \mathcal{Q}_f \partial \tilde{y} / \partial \mathbf{t} = -\mathcal{P}_f \tilde{y}. \end{cases} \quad (11b)$$

where  $\hat{s}(\tilde{x}, H(\tilde{x}))$  and  $\hat{f}(\tilde{y})$  represent the reduced and boundary layer systems, respectively.

*Proof.* First, we consider  $\varepsilon$  to be significantly small such that the velocity of  $\dot{z} \propto (1/\varepsilon)$  behaves instantaneously fast. Thus, for  $\varepsilon \approx 0$ , the fast dynamics in (8b) quickly reaches a *quasi-steady state* given the instantaneous fast dynamics  $h(x) = \text{col}(h_i(x))$ ,  $\forall i \in \mathbb{R}_i^n$ . We further define  $y = \text{col}(y_i)$ ,  $\forall i \in \mathbb{R}_i^n$  as the error between the *actual* fast dynamics and the quasi-steady state:  $y \triangleq \text{col}(z^* - h(x))$ . Moreover, to facilitate later applying Lyapunov theory, we express the system states using their incremental variables  $\tilde{z}^* = z^* - \bar{z}^*$ ,  $\tilde{y} = y - \bar{y}$  and  $\tilde{x} = x - \bar{x}$ . Therefore, when expressed in terms of incremental states, the *actual* fast dynamics are given by  $\tilde{z}^* \triangleq \tilde{y} + h(\tilde{x} + \bar{x}) - h(\bar{x}) = \tilde{y} + H(\tilde{x})$ , and we express the two time-separated systems in (9) as:

$$\dot{\tilde{x}} = s(\tilde{x}, \tilde{y} + H(\tilde{x})), \quad \text{and} \quad \varepsilon \frac{\partial(\tilde{y} + H(\tilde{x}))}{\partial \mathbf{t}} = f(\tilde{x}, \tilde{y} + H(\tilde{x})). \quad (12)$$

Under the stretched time-scale  $\mathbf{t} = (t/\varepsilon)$ —where  $t$  is the time when  $\varepsilon \approx 0$ —the two time-separated systems in (12) can be written as the *singular perturbation problem* in (11), divided into the reduced system (11a) and the boundary layer system (11b). Under this stretched time-scale the slow dynamics instantaneously attains a quasi-steady state as the fast dynamics are considered instantaneously fast, implying that  $\tilde{y} \approx 0$  in the reduced system. Furthermore, if Assumption 4 holds, the slow states entering the boundary layer are considered frozen variables, causing  $\tilde{x} = 0$  and  $\tilde{y} = 0$ , such that  $H(\tilde{x}) = 0$  in the boundary layer system (11b).  $\square$

### C. Stability Analysis

The following theorem analyzes the stability of the closed-loop DC microgrid in (5), presented as singular perturbed system in (11).

**Theorem 2.** (Exponential Stability of the Singularly Perturbed system). *Consider the singular perturbed system in (11) and suppose that  $\Omega(\tilde{v})$  and  $\Gamma(\tilde{v})$  are strictly monotonically increasing in  $\tilde{v}$ . Let*

$$\begin{aligned} K_1 &\triangleq [\mathbb{I} + k\mathcal{L}]^{-1}, & K_2 &\triangleq [\mathcal{L}K_1\mathcal{L}]^{-1}\mathcal{L}K_1. \\ K_4 &\triangleq -\frac{1}{2}[\mathbb{I} + \Lambda K_3^\top], & K_3 &\triangleq [\mathcal{K}_v(K_1 - K_1\mathcal{L}K_2 - \mathbb{I})], \\ \mathcal{M}_s(x) &\triangleq \begin{bmatrix} \mathcal{P}_x \hat{x} - \kappa_1 [\mathbb{I} + \Lambda K_3^\top] \omega(v) \\ \mathcal{B}_v \omega(v) \end{bmatrix}, & x &\triangleq \begin{bmatrix} \hat{x} \\ v \end{bmatrix}, \end{aligned} \quad (13)$$

and  $\mathcal{B}^*$  be the maximum eigenvalue of  $K_4^\top R^G R^G K_4 \omega'_{\max}$  for  $\omega'_{\max} = \max(\partial \omega(v) / \partial v)$ . If  $\mathcal{M}_s(x)$  is strictly monotonically increasing and the reduced system in (9) satisfies the following matrix inequality

$$\mathcal{B}_v \succ \mathcal{B}^* \succeq K_4^\top R^G R^G K_4 \omega'(v), \quad (14)$$

then, there exists  $\varepsilon^* > 0$  such that for all  $\tau_d \ll \varepsilon < \varepsilon^*$  the system in (9) is globally exponentially stable under the following bound:

$$-(x - \bar{x})^\top [\mathcal{M}_x(x) - \mathcal{M}_x(\bar{x})] \leq -\Upsilon \|\tilde{x}\|^2, \quad \Upsilon \in \mathbb{R}_{>0}. \quad (15)$$

*Proof.* From the dynamics of the singularly perturbed system in (11), we propose the following Lyapunov candidates for the the reduced system;  $V_s$ , and for the boundary layer system;  $W_f$ .

$$V_s(\tilde{x}) = \frac{1}{2} \tilde{x}^\top \mathcal{Q}_s \tilde{x} + \int_0^{\tilde{v}} \Omega^\top(\sigma) \tau d\sigma \geq 0, \quad (16a)$$

$$W_f(\tilde{y}) = \frac{1}{2} \tilde{y}^\top \mathcal{Q}_f \tilde{y} \geq 0, \quad (16b)$$

where  $\mathcal{Q}_s$ ,  $\mathcal{Q}_f$ , and  $\Omega(\cdot)$  are defined in (10). As  $\mathcal{Q}_f$  is a positive-definite matrix,  $W_f > 0$ ,  $\forall \tilde{y} \neq 0$ , and is radially unbounded. Moreover,  $\mathcal{Q}_s \succ 0$  ensures that the first quadratic term of (16a) is positive. Examining the sign of the integral part in (16a),  $\Omega(\tilde{v})$  is defined in Theorem 1 as a strictly monotonically increasing function in  $\tilde{v}$ . Accordingly, when multiplied by the increment of the curve ( $\sigma$ ), the integral is guaranteed to be positive for all  $\tilde{v}$ . As a result,  $V_s$  is positive for all  $\forall \tilde{v} \neq 0$ , and radially unbounded.

The time derivative of the Lyapunov function associated with the reduced system is then obtained as follows:

$$\begin{aligned} \dot{V}_s(\tilde{x}) &= \nabla^\top V_s(\tilde{x}) \dot{\tilde{x}} \\ &= -\tilde{x}^\top \mathcal{P}_s \tilde{x} + \tilde{x}^\top \kappa_1 \Omega(\tilde{v}) - \Omega^\top(\tilde{v}) \Gamma(\tilde{v}) \\ &\quad - \Omega^\top(\tilde{v}) \mathcal{B}_v \tilde{v} + \Omega^\top(\tilde{v}) K_3 \Lambda \kappa_1^\top \tilde{x} \\ &= -(x - \bar{x})^\top [\mathcal{M}_x(x) - \mathcal{M}_x(\bar{x})] - \Omega(\tilde{v})^\top \Gamma(\tilde{v}) \leq 0 \\ &= -(x - \bar{x})^\top [\mathcal{M}_x(x) - \mathcal{M}_x(\bar{x})] \leq 0 \end{aligned} \quad (17)$$

In the above derivation, the structure of the reduced system has been modified so that the Lyapunov function is solely a function of the slow states. Specifically, the integral controller dynamics in (11a) depends on the instantaneous fast dynamics  $H(\tilde{x})$ . However, solving  $\varepsilon \dot{\tilde{z}}^* = f(\tilde{x}, \tilde{z}^*)$  for  $\varepsilon \approx 0$  yields a closed-form expression of the instantaneous fast dynamics given as a function of the slow state  $\tilde{I}^G$ . Hence,  $H(\tilde{x}) = K_2 \Lambda \tilde{I}^G$ , allowing the dynamics of the integral controller to be expressed as:

$$\tau \dot{\tilde{v}} = -\Gamma(\tilde{v}) + K_3 \Lambda \tilde{I}^G - \mathcal{B}_v \tilde{v},$$

with  $K_2$  and  $K_3$  defined in (13). Moreover,  $\mathcal{P}_s$  is a positive-definite matrix (see (10)) and the first quadratic term in the second equality in (17) is non-positive. Furthermore,  $\Omega(\tilde{v})$  and  $\Gamma(\tilde{v})$  are monotonically increasing in  $\tilde{v}$ , ensuring that their product is positive such that  $-\Omega(\tilde{v})^\top \Gamma(\tilde{v}) \leq 0$ . Consequently,  $\dot{V}_s(\tilde{x}) \leq 0$  and the Lyapunov function is guaranteed to be decreasing along the trajectories of the reduced system, if and only if  $\mathcal{M}_s(x)$  is monotonically increasing, that is if

$$\tilde{x}^\top (\mathcal{M}_x(x) - \mathcal{M}_x(\tilde{x})) \geq 0 \Leftrightarrow \frac{1}{2} \left[ \frac{\partial \mathcal{M}_x(x)}{\partial x} + \frac{\partial \mathcal{M}_x(x)}{\partial x}^\top \right] \succ 0.$$

Computing the symmetric part of  $\frac{\partial \mathcal{M}_x(x)}{\partial x}$  then gives

$$\left. \frac{\partial \mathcal{M}_x}{\partial x} \right|_{\text{sym}} = \begin{bmatrix} R^G & 0 & 0 & K_4 \omega'(v) \\ 0 & R^E & 0 & 0 \\ 0 & 0 & G^{\text{cte}} & 0 \\ \omega'(v) K_4^\top & 0 & 0 & \mathcal{B}_v \omega'(v) \end{bmatrix}, \quad (18)$$

with  $\omega'(v) = \partial \omega(v) / \partial v$  and  $K_4$  defined in (13). Applying the Schur Complement to (18) provides the following inequality conditions for the matrix to be positive-definite:

$$\begin{aligned} \mathcal{B}_v \omega'(v) - \omega'(v) H^\top R^{G^{-1}} K_4 \omega'(v) &\succ 0, \\ \mathcal{B}_v &\succ K_4^\top R^{G^{-1}} K_4 \omega'(v). \end{aligned}$$

where the last inequality follows from multiplying the previous condition by the inverse of  $\omega'(v)$ . Given the sigmoid nature of  $\omega(v)$  in (3a), the nonlinear function is bounded by  $-1 \leq \tanh(\cdot) \leq 1$ , such that  $0 < \omega'(v) \leq \omega'_{\max}$ , which implies that  $\mathcal{B}_v$  can be chosen to be greater than a *constant* value  $\mathcal{B}_v^*$ , defined as the largest eigenvalue of  $K_4^\top R^{G^{-1}} K_4 \omega'_{\max}$ , with  $\omega'_{\max} = \mathbb{1}$ , which is indeed the condition in *Theorem 2*. Accordingly, we conclude upon global asymptotic stability, provided that the stability condition in (14) is satisfied. Furthermore, to guarantee G.E.S. we need to find an upper bound of the Lyapunov function  $V_s(\tilde{x}) \leq c \|\tilde{x}\|^2$ . Exploiting the fact that  $\Omega(\tilde{v})$  adheres to the Lipschitz condition, we contain the value of the integral as follows

$$\int_0^{\tilde{v}} [\Omega(\sigma)]^\top \partial \sigma \leq L \int_0^{\tilde{v}} \sigma \partial \sigma,$$

for some scalar  $\sigma > 0$  and  $L = 1$  is the Lipschitz constant. Thus,  $V_s(\tilde{x}) \leq V_1(\tilde{x})$  with  $V_1(\tilde{x}) \triangleq \frac{1}{2} \tilde{x}^\top Q_s \tilde{x} + \frac{1}{2} L \tilde{v} = \frac{1}{2} \tilde{x}^\top Q_s^* \tilde{x} \leq \Phi \|\tilde{x}\|^2$  and  $Q_s^* \triangleq \text{bdiag}\{Q_s, L\} \succ 0$ , with  $\Phi$  being the maximum eigenvalue of  $Q_s^*$ . Hence, we have

$$V_s(\tilde{x}) \leq \Phi \|\tilde{x}\|^2. \quad (19)$$

Finally, using (19) and (15), we conclude upon G.E.S. of the reduced system with a convergence rate given by  $\epsilon = 2 \frac{\Gamma}{\Phi}$ . Considering the Lyapunov function of the boundary layer system—given in (16b)—its time derivative is given as:

$$\frac{\partial W_f(\tilde{y})}{\partial t} = \nabla^\top W_f(\tilde{y}) \frac{\partial \tilde{y}}{\partial t} = -\tilde{y}^\top \mathcal{P}_f \tilde{y} \leq 0, \quad (20)$$

with  $\mathcal{P}_f$  defined to be positive definite in *Theorem 1*, ensuring that the final inequality in (20) holds. Accordingly, the singularly perturbed system in (11) satisfies all conditions given in *Theorem 11.4* in [25] and *Theorem 2*, and the system in (5) is globally exponentially stable as there exists a  $\epsilon^* > 0$  for all  $\tau_p \ll \tau_d \ll \epsilon < \epsilon^*$ .  $\square$

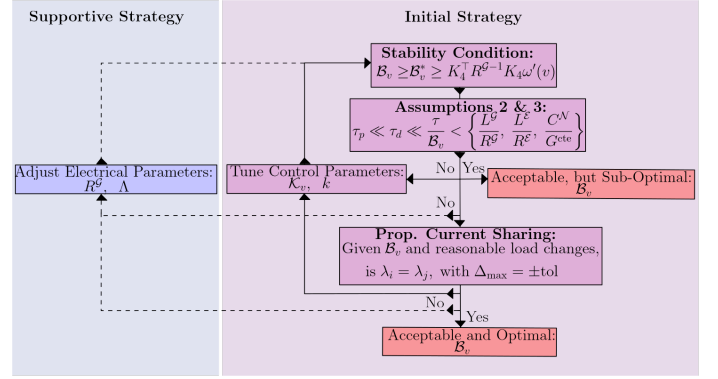


Fig. 2: Practical guidelines for stability and proportional current sharing

#### D. Practical Guidelines for Stability Guarantees

The previous subsection concludes that the system exponentially converges to a steady state when a sufficient time-scale separation is imposed for the nested control loops—following *Assumption 2*—provided that there exists a *permanent* leakage term in the integral controller with a value that satisfies the stability condition in (14). However, *Remark 1* indicates that any active leakage term introduced in the integral controller dynamics in (5d) inhibits *strict* proportional current sharing at steady state. Accordingly, this subsection proposes some tuning guidelines and parameter settings—visualized in Fig. 2—aimed at; (i) guaranteeing that the stability condition holds  $\forall t \in \mathbb{R}_{\geq 0}$ , (ii) preserving a sufficient time-scale separation, and (iii) minimizing  $\mathcal{B}_v$  to ensure that, at the converged equilibrium, the generated currents deviate by no more than  $\pm \text{tol}$  from the *optimal* equilibrium where *strict* proportional current sharing is satisfied—further referred to as *practical* proportional current sharing.

**Assumption 5.** *The proposed evaluation of the time-scales relies on the approximation where the convergence rate of each state can be defined by the ratio of inertia to damping  $\tau_i = \mathcal{I}_i / \mathcal{D}_i$ , provided that sufficient damping is introduced in the associated system dynamics.*

**Remark 2.** *When the state under consideration exhibits relatively strong damping, we let Assumption 5 hold. However, when the dynamical state exhibits negligible or non-permanent damping, the time constant is defined by the parameter multiplying the time-varying state.*

The primary objective is to determine a  $\mathcal{B}_v \geq \mathcal{B}_v^*$  that satisfy (14) in *Theorem 2*. However, based on the stability analysis and the resulting system modifications, the updated time constant of the integral controller is  $\tau / \mathcal{B}_v$ —in accordance with *Assumption 5*. Consequently, an elevated value of  $\mathcal{B}_v$  may both diminish *strict* proportional current sharing and violate the required time-scale separation. Per *Theorem 2*,  $\mathcal{B}_v$  depends on the generator resistances ( $R^G$ ), rated currents ( $\Lambda$ ), the integral gain ( $K_v$ ), and the positive control gain ( $k$ ). Therefore, the initial (and preferable) strategy in Fig. 2, solely relies on tuning the controller ( $K_v$  and  $k$ ) to satisfactorily reduce the value of  $\mathcal{B}_v^*$ . In this case, the stability result is independent on any system parameters and the resulting G.E.S. certificate is *scalable*. However, if this controller tuning is insufficient in satisfying the stability condition and time-scale separation, there exists a supportive strategy that includes modifying the respective system parameters, albeit at the cost of generating a more conservative and system dependent stability certificate. Finally, for the *practical* proportional current sharing

objective, an acceptable  $\mathcal{B}_v$  may be *sub-optimal* if the generated currents deviate beyond the allowable tolerance. Depending on the practical engineering objectives, further tuning of the controller and modifying the system parameters is always possible, albeit at the expense of reducing the generality of the resulting configuration.

**Remark 3.** *It is important to note that, given the already high-speed nature of DC systems, very fast communication rates are essential to uphold this time-scale separation. Interestingly, recent advancements in electric intelligent vehicular technology have led to the development of more reliable and faster communication protocols to enhance the safety and performance of autonomous vehicles. To deal with this growing demand for data transmission, the Controller Area Network with Flexible Data Rate (CAN-FD) communication protocol has been introduced, supporting data rates of up to 8 Mbps [26]–[28]. Although potentially limited to some (geographically-contained) applications, the CAN-FD protocol provides sufficient communication rates supporting the proposed time-scales proposed in this research.*

#### IV. CASE STUDIES

The proposed control framework is tested by means of time-domain simulations in MATLAB/Simulink on a 48-volt DC network. The microgrid admits the dynamics in (1), powered by 4 DGs, interconnected electrically and through communication links according to the arbitrary interconnection patterns depicted in Fig. 3. The specifications of the generators, loads, and power lines are given in Table I. For the initial system configurations, the selected control parameters—chosen to satisfy *Assumption 2*—are listed below, with the time constants specified in seconds.

$$\begin{aligned} \tau &= \text{diag}(1e^{-3}), \quad \tau_p = \text{diag}(0.01e^{-3}), \quad \tau_d = \text{diag}(0.1e^{-3}), \\ \mathcal{K}_v &= \text{diag}(V^*), \quad \mathcal{B}_v = 0, \quad \alpha = V_{\max}, \quad k = 10, \quad b = 5. \end{aligned} \quad (21)$$

For the voltage containment objective, the maximum allowed voltage deviation from the nominal voltage,  $V_n = 48V$ , are 5%;  $V_{\max} = 1.05[\text{p.u}]$  and  $V_{\min} = 0.95[\text{p.u}]$ , and for *practical* proportional current sharing we permit an acceptable  $\pm 5\%$  deviation from the *optimal* steady state operating point where *strict* proportional current sharing is satisfied.

##### A. Case Study 1: Control Performance under Stability Constraints

In the following case studies, we aim to identify an acceptable controller tuning and equipment sizing that guarantee system convergence to a steady state attaining *near-optimal* DC MG operations, in which both voltage containment and *practical* proportional current sharing are satisfied. Moreover, we impose various system events to evaluate the controller performance under both minor and more extreme load variations, as well as testing the robustness and stable plug-and-play capability under various network reconfiguration events—all imposed system events are defined in Fig. 4.

##### 1) Initial System Configurations

Employing the initial system configurations—given in Table I and (21)—the DC MG is preliminary tested without any stability guarantees; thus,  $\mathcal{B}_v = 0$ . The system response in Fig. 4(a) show that the the DG voltages are always contained, and during more significant load changes some of the DG voltages reach their saturation limits, activating the *non-permanent* leakage  $\rho(v)$ , depicted in Fig. 4(b). Although the simulations in Fig. 4(c) indicate *near-optimal* steady

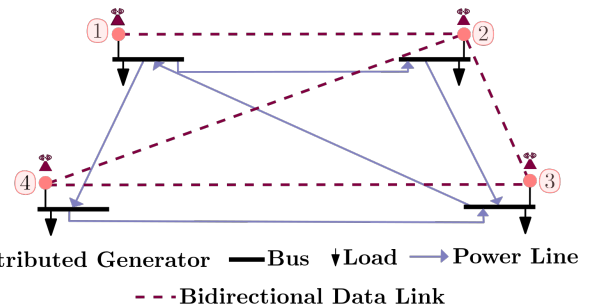


Fig. 3: Case-specific DC microgrid with 4 DGs.

TABLE I: Electrical Specifications for Case-Specific MG; resistance ( $R$ ) and inductance ( $L$ ) values are given in per unit (p.u) on a  $0.15\Omega, 300\mu H$  base.

Generator specifications; $i \in \mathcal{G}$				
$I_i^{\text{rated}}$ [A]	12	4	8	8
$R_i^{\mathcal{G}}$ [p.u], $L_i^{\mathcal{G}}$ [p.u]	0.5	0.4	0.55	0.6
Load specifications; $k \in \mathcal{N}$				
$C_k^{\mathcal{N}}$ [F]	$22 \times 10^{-3}$			
$1/G_k^{\text{cte}}$ [ $\Omega$ ]	40	30	30	30
$I_k^{\text{cte}}$ [A]	1	1.2	0.8	1
Power lines specifications; $j \in \mathcal{E}$				
$R_j^{\mathcal{E}}$ [p.u], $L_j^{\mathcal{E}}$ [p.u]	1	2	2	1

state convergence—for *strict* proportional current sharing, the system should exhibit a response where the integration errors approach zero in steady state—stability is not guaranteed, as the conditions in *Theorem 2* are not satisfied. To guarantee stability under these initial system configurations, the *permanent* leakage  $\mathcal{B}_v$  must be chosen at least 349.5. However, this values violates *Assumption 2*, as  $(\tau/\mathcal{B}_v) = 2.86\mu \ll \tau_p, \tau_d$  meaning that the inner-loop controller operates at a faster time-scale than the outer-loop controller.

##### 2) Stable System Configurations

Accordingly, to evaluate the DC MG under sufficient stability conditions, it is first necessary to carefully determine an acceptable  $\mathcal{B}_v$ -value. Unfortunately, for the initial system specifications, it appears infeasible to identify a set of control parameters that satisfy the required stability conditions. As a result, we apply the controller to a distinct version of our case-specific system following the supportive strategy in Section III-D. Specifically, we adjust the generators base resistance up to  $0.2\Omega$  and lowered  $\mathcal{K}_v$  to 1, resulting in  $\mathcal{B}_v = 2.54$ , which aligns with the appropriate time-scales for the decentralized controller ( $\tau/\mathcal{B}_v = 0.34e^{-1} > \tau_p, \tau_d$ ). Thus, the simulation results depicted in Fig. 4 (d)-(f) feature the system response of the DC MG under a controller tuning—and equipment sizing—satisfying *Theorem 2* and *Assumption 2*.

Fig. 4(d) illustrates that the voltages remain contained during all system events. However, saturation is never reached due to the active *permanent* leakage, and the *non-permanent* leakage function remains deactivated throughout the simulation, as depicted in Fig. 4(e). Moreover, the active *permanent* leakage—combined with arguably some extreme load variations—prevents complete convergence to *strict* proportional current sharing in steady state with high percentage deviation—up to 56%—given by:  $\Delta_{\max} = \left[ \frac{(\lambda_i - \Lambda_i) I_i^{\mathcal{G}}}{\lambda_i} \right]_t$ , measured for each time-step  $t$ —see Fig. 4(f). That Said, the simulation results demonstrate the controllers robust plug-and-play capability, maintaining stability despite topological changes in the electrical network.

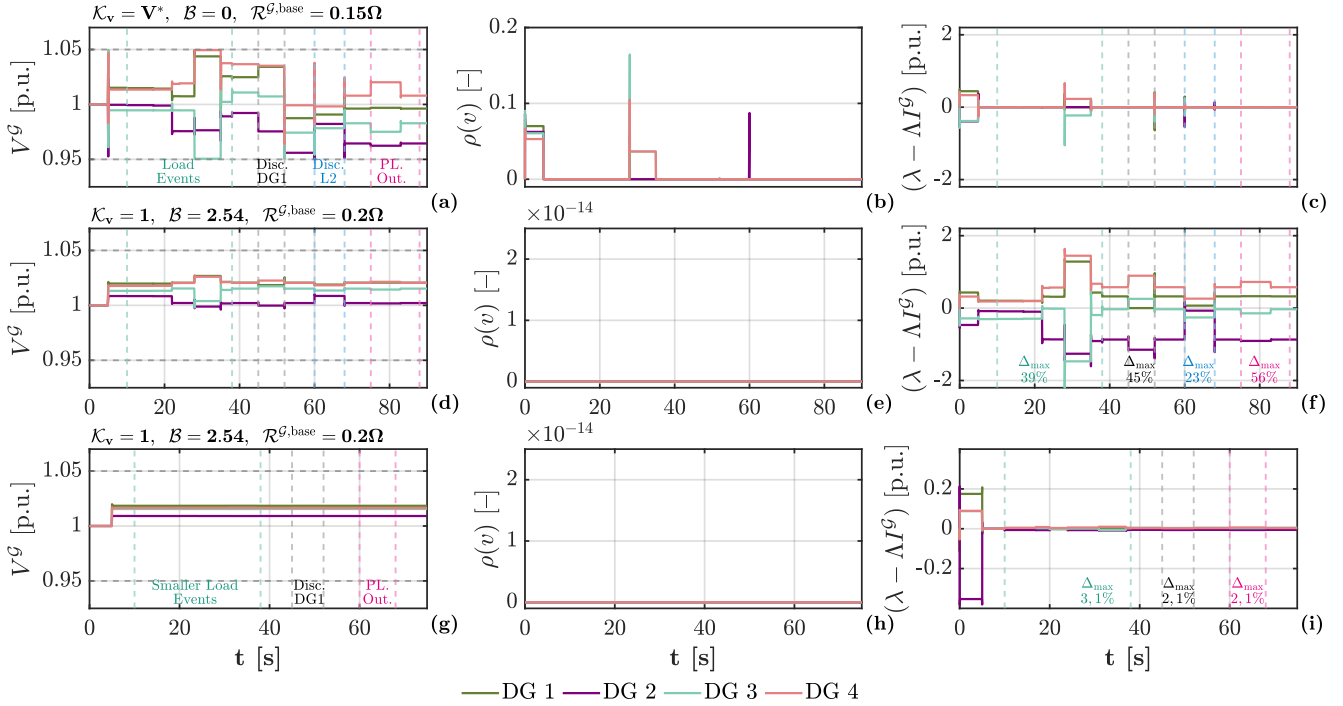


Fig. 4: Simulation results for Case Study 1.1 (a)-(c) (first row), Case Study 1.2 (d)-(f) (second row), Case Study 1.3 (g)-(i) (third row); (a), (d), and (g) generators voltages; (b), (e), and (h) *non-permanent* leakage function; (c), (f), and (i) integrations errors; Imposed load changes in Case Study 1 & 2:  $t=5$ : activation of distributed controller,  $t=10$ : Inc. $G_1^{\text{cte}}$  45%,  $t=17$ : Inc. $I_1^{\text{cte}}$  75%,  $t=22$ : Inc. $G_2^{\text{cte}}$  500% and Inc. $I_1^{\text{cte}}$  800%,  $t=24$ : Red. $I_4^{\text{cte}}$  35%,  $t=28$ : Inc. $G_3^{\text{cte}}$  900%,  $t=35$ : Red. $G_3^{\text{cte}}$  80%,  $t=38$ : Red. $I_3^{\text{cte}}$  90%; Imposed disconnections in Case Study 1&2:  $t \in [45,52]$  Disc. DG1,  $t \in [60,68]$  Disc. load 2,  $t \in [75,83]$  Disc. PL between load 3 and 4; Imposed load changes in Case Study 3:  $t=5$ : activation of distributed controller,  $t=10$ : Inc. $I_1^{\text{cte}}$  50%,  $t=17$ : Red. $I_4^{\text{cte}}$  13%,  $t=20$ : Red. $G_1^{\text{cte}}$  40%,  $t=24$ : Inc. $G_2^{\text{cte}}$  5%,  $t=31$ : Inc. $G_3^{\text{cte}}$  17%,  $t=37$ : Red. $I_3^{\text{cte}}$  45%,  $t=38$ : Red. $G_3^{\text{cte}}$  7%; Imposed disconnections in Case Study 3:  $t \in [45,52]$  Disc. DG1,  $t \in [60,68]$  Disc. PL between load 3 and 4.

### 3) Stable System Configurations and Practical Proportional Current Sharing

Aiming to ensure *practical* proportional current sharing, the system is now simulated under arguably more realistic load variations. Compared to the previous simulations—where load consumption was varied between a minimum of 35% and a maximum of 900%—the current study limits load changes to 50%, reflecting more realistic conditions for a low-voltage MG. We retain the parameter values from the previous study. The voltages depicted in Fig. 4(g) remain contained and the chosen value of the *permanent* leakage effectively dominates the *non-permanent* leakage function ( $\rho(v)$ ), as illustrated in Fig. 4(h). Furthermore, Fig. 4(i) demonstrates that *practical* proportional current sharing is consistently achieved within the allowable  $\pm 5\%$  tolerance. The results demonstrate that the controller consistently ensures stable and *near-optimal* operations, stabilizing to an equilibrium that satisfies both control objectives, regardless of any topological changes, and thus, supports practical PnP feasibility.

#### B. Case Study 2: Control Performance under Communication Delays

In this second case study, we simulate the case-specific DC MG with communication delays in the outer-loop controller—while keeping similar load conditions as in Case Study 1.3., including disconnecting DG1 and the power line outage. The objective is to evaluate the controllers ability to achieve consensus under realistic, assorted communication delays. Moreover, as suggested in [29], such time delays can be interpreted as a proxy for communication packet losses, thereby offering insight into the systems robustness under adverse communica-

tion conditions. In the primary scenario—depicted in Fig. 5 (a), (b), and (d)—DG2 communicates with a time-delay of 0.1ms, and DG4 with a delay of 0.2ms. These delays are selected to respect the time-scale separation necessary to guarantee G.E.S.. Fig. 5(a) and (b) illustrates that despite the communication delays, the system converges to the same steady-state values as in Fig. 4(g) and (i), with maximum deviation from *strict* current sharing remaining consistent with the previous result. However, comparing Fig. 5(c) and (d) indicates that under communication delays the transient response is slower, reflected in an extended rise time—defined as the interval from the onset of an event to the point where the system reaches its steady-state value. Nevertheless, the overall convergence time remains similar, likely due to the slow system dynamics unaffected by these very fast communication delays. Moreover, to evaluate system stability under more severe communication delays, we impose delays that violate the time-scale assumptions required to guarantee G.E.S. In Fig. 5(e) and (f), DG1 communicates with its neighbors with a 2ms delay, DG2 remains at 0.1ms, and DG4 with 0.2s. The system response indicates that these delays destabilizes the system, as the generator voltages stabilizing to an orbit. Notably, however, the voltages remain contained within a limit cycle due to the nonlinear control input of the inner-loop controller.

TABLE II: Equilibrium of  $\lambda$  and  $\zeta$  with  $\mathcal{B}_c = 1e^{-4}$

$\lambda_1$	$\lambda_2$	$\lambda_3$	$\lambda_4$	$\zeta_1$	$\zeta_2$	$\zeta_3$	$\zeta_4$
0.3560	0.3560	0.3560	0.3560	-0.0638	0.0584	0.0042	0.0012

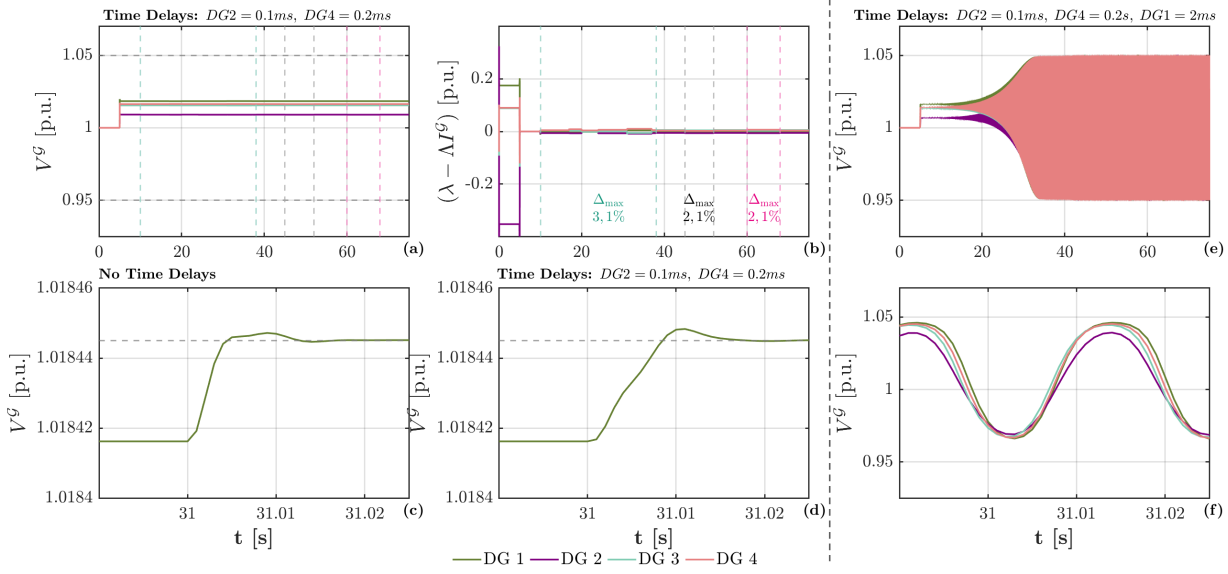


Fig. 5: Case-specific microgrid under time delays; (a)(b)(d) system response under time delays that respect the time-scale separation: (a)(d) generator voltages, (b) integration error; (c) generator voltages under normal operations; (e)(f) generator voltages under time delays that violates the time-scale separation.

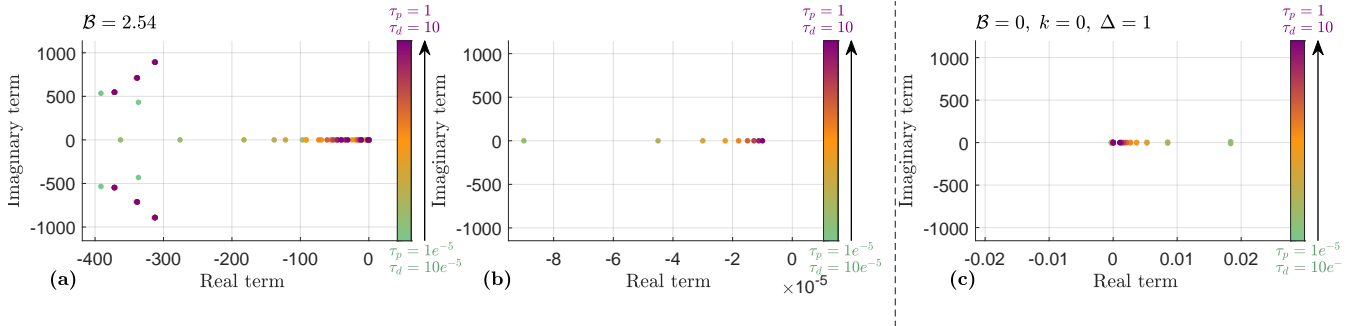


Fig. 6: Eigenvalues of the case-specific MG for a parametric sweep of  $\tau_p, \tau_d$ : (a) and (b) eigenvalues under acceptable control parameters (and associated electrical specifications), (b) detailed plot around zero; (c) eigenvalues under unstable tuning conditions (detailed plot around zero).

### C. Case Study 3: Small-Signal Stability Analysis

Finally, we conduct a small-signal stability analysis to determine whether a less conservative stability bound exists, thereby expanding the area of application of the results in this research. Given that large-signal stability is preserved within substantial margins—characterized by significant time-scale separation—we explore the possibility of operating the system under reduced *large-signal* stability margins for slower communication rates. We begin by noting that the outer-loop dynamics depend on the cyber-network topology defined by the Laplacian matrix, which inherently yields a zero eigenvalue due to its mathematical properties. Hence, to properly evaluate the closed-loop systems eigenvalues from a small-signal stability perspective, a small constant leakage,  $B_\zeta$ , is introduced in the  $\zeta$ -coordinate in (5f) to add dissipation and shift the zero eigenvalue further into the left-half plane. That said, it is important to note that this leakage term affects the steady state operations of the system—particularly the controller ability to determine a common consensus value of the dual communication state  $\zeta$ . As discussed in Remark 1, the *optimal* equilibrium for *strict* proportional current sharing is defined when  $\lambda_i \approx \lambda_j$  and  $\zeta_i \approx \zeta_j$ . Accordingly, we select  $B_\zeta = 1e^{-4}$  as the maximum allowed value before hindering proportional current sharing—the resulting equilibrium values for  $\lambda$  and  $\zeta$  are detailed in Table II. To examine

the impact of decreasing the communication rates, we plot the eigenvalues of the case-specific DC MG for a parametric sweep of the communication time constants  $\tau_p$  and  $\tau_d$  while keeping the *permanent* leakage value:  $B=2.54$ . The resulting eigenvalues are given in Fig. 6 (a)-(b). From Fig. 6 (a), it is evident that reducing the communication rates brings the system closer to unstable operations as the eigenvalues tend towards positive real values. However, the eigenvalues never become positive, and the system is stable from a small-signal perspective. Furthermore, the small-signal stability assessment is also used to reinforce the findings of the large-signal stability analysis. Fig. 6(c) maps the eigenvalues of the closed-loop DC MG without careful tuning that guarantees overall stability;  $B_v = 0$ ,  $k = 0$ , and decreasing the allowable voltage range ( $\Delta = 1$ ). The resulting plot depicts positive real eigenvalues, and the system is unstable.

**Remark 4.** Note that in Fig. 6(c), eigenvalues shift toward negative real values when communication rates are significantly decreased, even with zero permanent leakage. This suggests a *converse time-scale separation*, where the outer-loop controller is slower than the rest of the system, removing the stability constraints on the permanent leakage—which is addressed in [30] and further explored in future work.

## V. CONCLUSION AND FUTURE WORK

In conclusion, this paper derives a global exponential stability certificate for a DC microgrid with nonlinear nested distributed control configurations—originally proposed in [2] and later modified in [1]. Building upon the methodology used in [3], we express the closed-loop system as a singularly perturbed problem, separating the outer-loop dynamics (secondary controller with inherent communication technologies), and the inner-loop dynamics (primary controller and electrical system) by sufficient time-scales. Using Lyapunov arguments, this paper establishes global exponential convergence to a steady state, provided that a *permanent* leakage term of sufficient magnitude is included in the primary controller. To guarantee *practical* proportional current sharing, some practical guidelines are proposed to reduce the *permanent* leakage within the allowable stability range, while the nonlinear inner-loop controller continuously ensures voltage containment. While the structure of the stability proof is *scalable*, the resulting stability guarantees depend on carefully selected control parameter and some electrical specifications, thereby limiting the scalability and general applicability of the result. Consequently, future work should aim to generalize some worst-case tuning conditions that ensure stability (and proper time-scale separation) under the applied controller parameters for expandable systems across a range of initial system configurations. However, this may compromise proportional current sharing considerably, and the selection of the *permanent* leakage should be guided by the intended engineering objective: either *scalable* and stable system guarantees for highly diverse networks—however, with possibly reduced proportional power sharing performance—or, stable and *near*-optimal operations—albeit limited to a more case-specific system. Furthermore, the theoretical large-signal stability guarantees rely on relatively fast communication rates, making the current configuration more applicable to smaller, localized systems where such communication speeds are feasible. Finally, the stability results and control performance are validated on a case-specific DC microgrid under appropriate controller tuning and parameter settings. The results demonstrate continuous voltage containment and *practical* proportional current sharing under realistic load variations and topological changes. A small-signal stability analysis provides guidelines for relaxing the time-scale separation. While operating outside the large-signal stability conditions is possible, compensatory measures such as additional studies and extended time-domain simulations are required. The case studies also indicate stable and *near*-optimal operations under communication delays that remain within the assumed time-scale separation,

## REFERENCES

- [1] C. Skaga, B. Abdolmaleki, and G. Bergna-Diaz, "Stability of a distributed controller for optimal current sharing and voltage containment in dc microgrids," *IEEE GPECOM*, 2024.
- [2] B. Abdolmaleki and G. Bergna-Diaz, "A nonlinear control framework for optimal load-sharing and voltage containment in dc networks," *IEEE Transactions on Power Systems*, vol. 38, no. 1, pp. 976–979, 2023.
- [3] B. Abdolmaleki, J. Simpson-Porco, and G. Bergna-Diaz, "Distributed optimization for reactive power sharing and stability of inverter-based resources under voltage limits," *IEEE Transactions on Smart Grid*, vol. 15, no. 2, pp. 1289–1303, Mar. 2024.
- [4] F. Dörfler, J. W. Simpson-Porco, and F. Bullo, "Breaking the hierarchy: Distributed control and economic optimality in microgrids," *IEEE Transactions on Control of Network Systems*, vol. 3, no. 3, pp. 241–253, 2016.
- [5] G. Michos, P. R. Balddivieso-Monasterios, G. C. Konstantopoulos, and P. A. Trodden, "Robust two-layer control of dc microgrids with fluctuating constant power load demand," *IEEE Transactions on Control of Network Systems*, vol. 11, no. 1, pp. 427–438, 2024.
- [6] A. A. Tavagnutti, S. Bertagna, M. Dalle Feste, M. Chiandone, D. Bosich, V. Bucci, and G. Sulligoi, "The coordinated power control of flexible dc microgrids in sustainably optimized yacht marinas," *Energies*, vol. 17, no. 2, 2024.
- [7] E. Nivolianiti, Y. L. Karnavas, and J.-F. Charpentier, "Energy management of shipboard microgrids integrating energy storage systems: A review," *Renewable and Sustainable Energy Reviews*, vol. 189, p. 114012, 2024.
- [8] L. Xu, J. M. Guerrero, A. Lashab, B. Wei, N. Bazmohammadi, J. C. Vasquez, and A. Abusorrah, "A review of dc shipboard microgrids—part i: Power architectures, energy storage, and power converters," *IEEE Transactions on Power Electronics*, vol. 37, no. 5, pp. 5155–5172, 2022.
- [9] M. S. Sadabadi, N. Mijatovic, and T. Dragičević, "A robust cooperative distributed secondary control strategy for dc microgrids with fewer communication requirements," *IEEE Transactions on Power Electronics*, vol. 38, no. 1, pp. 271–282, 2022.
- [10] L. Xiong, X. Liu, Y. Liu, and F. Zhuo, "Modeling and stability issues of voltage-source converter-dominated power systems: A review," *CSEE Journal of Power and Energy Systems*, vol. 8, no. 6, pp. 1530–1549, 2022.
- [11] F. Gao, R. Kang, J. Cao, and T. Yang, "Primary and secondary control in dc microgrids: a review," *Journal of Modern Power Systems and Clean Energy*, vol. 7, no. 2, pp. 227–242, 2019.
- [12] L. Meng, Q. Shafiee, G. F. Trecate, H. Karimi, D. Fulwani, X. Lu, and J. M. Guerrero, "Review on control of dc microgrids and multiple microgrid clusters," *IEEE Journal of Emerging and Selected Topics in Power Electronics*, vol. 5, no. 3, pp. 928–948, 2017.
- [13] P. Nahata, M. S. Turan, and G. Ferrari-Trecate, "Consensus-based current sharing and voltage balancing in dc microgrids with exponential loads," *IEEE Transactions on Control Systems Technology*, vol. 30, no. 4, pp. 1668–1680, 2021.
- [14] M. Tucci, L. Meng, J. M. Guerrero, and G. Ferrari-Trecate, "Stable current sharing and voltage balancing in dc microgrids: A consensus-based secondary control layer," *Automatica*, vol. 95, pp. 1–13, 2018.
- [15] T. Dragičević, X. Lu, J. C. Vasquez, and J. M. Guerrero, "Dc microgrids—part i: A review of control strategies and stabilization techniques," *IEEE Transactions on Power Electronics*, vol. 31, no. 7, pp. 4876–4891, 2016.
- [16] C. Skaga, M. S. Sadabadi, and G. Bergna-Diaz, "Dc microgrids with nested nonlinear distributed control: Scalable large-signal stability and voltage containment," *arXiv preprint arXiv:2602.14725*, 2026.
- [17] J. Zhao and F. Dörfler, "Distributed control and optimization in dc microgrids," *Automatica*, vol. 61, pp. 18–26, 2015.
- [18] C. D. Persis, E. Weitenberg, and F. Dörfler, "A power consensus algorithm for dc microgrids," *Automatica*, vol. 89, pp. 364–375, 2018.
- [19] S. Trip, M. Cucuzzella, X. Cheng, and J. Scherpen, "Distributed averaging control for voltage regulation and current sharing in dc microgrids," *IEEE Control System Letter*, vol. 3, no. 1, pp. 174–179, 2019.
- [20] M. Cucuzzella, S. Trip, C. D. Persis, X. Cheng, A. Ferrara, and A. van der Schaft, "A robust consensus algorithm for current sharing and voltage regulation in dc microgrids," *IEEE Transaction on Control System Technology*, vol. 27, no. 4, pp. 1583–1595, 2019.
- [21] D. E. Olivares, A. Mehrizi-Sani, A. H. Etemadi, C. A. Cañizares, R. Iravani, M. Kazerani, A. H. Hajimiragha, O. Gomis-Bellmunt, M. Saeedifard, R. Palma-Behnke, G. A. Jiménez-Estévez, and N. D. Hatziaargyriou, "Trends in microgrid control," *IEEE Transactions on Smart Grid*, vol. 5, no. 4, pp. 1905–1919, 2014.
- [22] X. Wu, C. Shen, and R. Iravani, "Feasible range and optimal value of the virtual impedance for droop-based control of microgrids," *IEEE Transactions on Smart Grid*, vol. 8, no. 3, pp. 1242–1251, 2017.
- [23] S. D'Arco and J. A. Suul, "Equivalence of virtual synchronous machines and frequency-droops for converter-based microgrids," *IEEE Transactions on Smart Grid*, vol. 5, no. 1, pp. 394–395, 2014.
- [24] B. Abdolmaleki and G. Bergna-Diaz, "Distributed control and optimization of dc microgrids: A port-hamiltonian approach," *IEEE Access*, vol. 10, pp. 64 222–64 233, June 2022.
- [25] H. K. Khalil, *Nonlinear systems*, 3rd ed. Prentice Hall, 2002.
- [26] H. Kim, W. Yoo, S. Ha, and J. Chug, "In-vehicle network average response time analysis for can-fd and automotive ethernet," *IEEE Transactions on Vehicular Technology*, vol. 72, no. 6, pp. 6916–6932, 06 2023.
- [27] S. Kang, J. Seong, and M. Lee, "Controller area network with flexible data rate transmitter design with low electromagnetic emission," *IEEE Transactions on Vehicular Technology*, vol. 67, no. 8, pp. 7290–7298, 08 2018.
- [28] R. de Andrade, M. M. D. Santos, J. F. Justo, L. R. Yoshioka, H.-J. Hof, and J. H. Kleinschmidt, "Security architecture for automotive communication networks with can fd," *Computers & Security*, vol. 129, p. 103203, 2023.
- [29] Y. Yu, G.-P. Liu, and W. Hu, "Coordinated distributed predictive control for voltage regulation of dc microgrids with communication delays and data loss," *IEEE Transactions on Smart Grid*, vol. 14, no. 3, pp. 1708–1722, 2023.
- [30] C. Skaga, M. S. Sadabadi, and G. Bergna-Diaz, "Large-signal stability guarantees for a scalable dc microgrid with nonlinear distributed control: The slow communication scenario," *arXiv preprint arXiv:2511.10380*, 2025.